J. Fluid Mech. (2006), *vol.* 547, *pp.* 105–113.
doi:10.1017/S0022112005007585 Printed in the United Kingdom

Note on the induced Lagrangian drift and added-mass of a vortex

By JOHN O. DABIRI

Graduate Aeronautical Laboratories & Bioengineering, California Institute of Technology, Pasadena, CA 91125, USA

(Received 3 August 2005 and in revised form 8 October 2005)

Darwin (1953) introduced a simple heuristic that relates the Lagrangian fluid drift induced by a solid body propagating in irrotational flow to its virtual- or added-mass. The force required to accelerate the solid body must also overcome this added-mass. An extension of Darwin's (1953) method to the case of vortices propagating in a real fluid is described here. Experiments are conducted to demonstrate the existence of an added-mass effect during uni-directional vortex motion, which is analogous to the effect of solid bodies in potential flow. The definition of the vortex added-mass coefficient is modified from the solid body case to account for entrainment of ambient fluid by the vortex. This modified coefficient for propagating vortices is shown to be equal in magnitude to the classical coefficient for a solid body of equivalent boundary geometry. An implication of these results is that the vortex added-mass concept can be used as a surrogate for the velocity potential, in order to facilitate calculations of the pressure contribution to forces required to set fluid into unsteady vortical motion. Application of these results to unsteady wake analyses and fluid–structure interactions such as vortex-induced vibrations is suggested.

1. Introduction

Darwin (1953) demonstrated that the virtual- or added-mass associated with a solid body propagating in an unbounded ideal fluid is manifested in the induced Lagrangian drift of flow around the body. The relationship between induced Lagrangian drift and added-mass can be quantified by considering the unidirectional motion of a body of volume V_B at speed U (where the direction of motion, taken in the following to be along the x-axis, coincides with the diagonal term of the added-mass tensor under consideration). As the body, starting upstream at $x \to -\infty$, passes through an infinite plane of Lagrangian particles at $x = 0$, a net downstream drift of the particles is induced (see figure 1 below). When the body has moved far downstream, i.e. $x \to \infty$, the volume V_D between the distorted Lagrangian plane and its original position is equal to the added-mass (per unit fluid density) of the body. More formally,

$$c_{xx} = \frac{V_D}{V_B} = \frac{1}{V_B U} \int_S \phi n_1 \, \mathrm{d}s, \tag{1.1}$$

where c_{xx} is the added-mass coefficient, ϕ is the velocity potential at the surface S of the body, and n_1 is the x-component of the unit normal vector directed into the body (Benjamin 1986). A proof of the relationship in (1.1) requires care in the order of integration and the manner in which the spatial limits are taken to infinity (cf. Lighthill 1956; Benjamin 1986; Yih 1997). However, recent work by Eames, Belcher &

Hunt (1994), Eames & Duursma (1997), Eames & Flór (1998), Bush & Eames (1998) and Eames (2003) has demonstrated that these subtleties are less relevant in the practical implementation of Darwin's (1953) concept.

A recent experimental study of geophysical dipole vortices suggested that the propagation of coherent vortical structures may also induce Lagrangian drift in the surrounding fluid, in a manner characteristic of the solid body added-mass effect (Eames & Flór 1998). However, measurements of the added-mass coefficient (1.1) from dye visualizations of the vortices were observed to deviate from the value for a solid body of equivalent boundary geometry in potential flow. The discrepancy was primarily attributed to entrainment of ambient fluid by the vortex.

Turner (1964) used an analytical model of an expanding spherical vortex in irrotational flow to demonstrate that, in the case of a vortex, the process of ambient fluid entrainment makes it impossible to define a finite volume of fluid exhibiting drift behaviour similar to that of a solid body. Instead, Lagrangian particles near the centreline of the body become entrained and therefore propagate downstream indefinitely at a velocity proportional to the volume growth rate of the vortex. This leads to a continual (i.e. not localized in time) increase in the drift volume V_D associated with the vortex, from which equation (1.1) would suggest a non-physical, infinite added-mass coefficient.

Since the vortex growth rate in the analytical model of Turner (1964) has to be specified *a priori*, that model cannot be used to directly infer the effect of ambient fluid entrainment on the vortex dynamics, or to suggest how the induced Lagrangian drift of fluid surrounding the vortex can be quantified in terms of an added-mass coefficient. Therefore, although hinted by these previous studies, the concept of a vortex added-mass effect and an associated added-mass coefficient has until now remained an unresolved proposition.

This paper describes an experimental investigation of vortex rings propagating unidirectionally, which is used to quantitatively relate the induced Lagrangian drift of fluid surrounding vortices with a well-defined vortex added-mass coefficient. Section 2 describes the experimental apparatus, measurement techniques, and method of analysis. Section 3 presents a comparison between the dynamics of the measured vortex flow and the potential flow behaviour examined by Darwin (1953) and others. A modified definition of the added-mass coefficient is presented in this section, which is sufficiently general to apply to solid bodies and fluid vortices with possibly time-dependent boundaries. The limitations of these results as well as their potential application to unsteady wake analyses and fluid–structure interactions such as vortex-induced vibrations is discussed in § 4.

2. Experimental and analytical methods

The induced Lagrangian drift and added-mass behaviour of vortex rings was investigated experimentally. A piston–cylinder apparatus submerged in a 60 cm height $\times$ 40 cm width $\times$ 110 cm length water tank created vortex rings with stroke length-to-diamater ratio (L/D) equal to 2.0 (cf. Dabiri & Gharib 2004). The boundary layer of starting flow emerging from the cylinder (inner radius = 1.27 cm) during a piston pulse rolled into a single vortex ring, which subsequently propagated downstream in the water tank under its self-induced velocity. The Reynolds number of the vortex ring flow was 1400 based on the cylinder exit diameter and piston velocity (nominally impulsive piston motion with 5.5 cm s^{-1} peak velocity), and 2000 based on the vortex ring circulation and kinematic viscosity of the water at room temperature.

Flow generated by the piston–cylinder apparatus was measured in a meridian symmetry plane using digital particle image velocimetry (DPIV, cf. Adrian 1991; Willert & Gharib 1991). A 30 Hz, 1024×1024 pixel CCD camera imaged the Mie scattering of an incident 532 nm Nd:YAG laser sheet from 13-micron neutrally buoyant particles seeded in the flow. The measurement window extended 15.7 cylinder radii in the streamwise direction downstream from the cylinder exit and 4.9 cylinder radii in the transverse direction from the axis of symmetry. The camera pixel resolution corresponds to a physical test section resolution of approximately 0.019×0.019 cm. Image pairs representing an 18 ms separation between laser pulses were interrogated with a window size of 32×32 pixels and 50 % overlap. Cross-correlation and velocity field calculations were accomplished using an in-house code on an Intel 2-GHz processor. Velocity measurements possess an uncertainty of 1 % to 2 %.

To determine the induced Lagrangian drift of flow surrounding the vortex ring as it propagated through the measurement window, the trajectories of approximately 2100 virtual particles in the flow downstream from the vortex generator were tracked quantitatively. The particles were initialized on 64 lines (representing planes in the axisymmetric flow) downstream of the vortex generator exit and oriented normal to the streamwise direction. The lines were spaced in 0.3 cm increments axially and extended to the radial extent of the measurement window.

Particle positions were updated according to the measured time-dependent Eulerian velocity field from DPIV and the known time interval between velocity field measurements (67 ms, i.e. twice the duration of each camera frame). When particles were advected to locations in the measurement field that did not coincide with a node of the DPIV velocity field, the particle velocity was determined from a cubic interpolation of the measured velocity field. The volume of fluid between the initial location of each plane and its final distorted position (i.e. after passage of the vortex ring) was calculated by assuming an axisymmetric geometry in accordance with the known flow configuration. Volume measurements possess a maximum uncertainty of 8 %.

For comparison with the vortex measurements, a similar particle advection technique was used to reproduce the Lagrangian trajectories induced by the passage of a solid sphere in irrotational flow. This flow has an exact solution given by

$$v_r = \mathrm{d}r/\mathrm{d}t = -(1 - a^3/r^3)\cos\theta, \tag{2.1}$$

$$v_\theta = r\,\mathrm{d}\theta/\mathrm{d}t = (1 + a^3/2r^3)\sin\theta, \tag{2.2}$$

where r is the radial coordinate, θ is the angular coordinate measured from the direction of oncoming flow (in the reference frame of the propagating sphere), and a is the sphere radius (Turner 1964).

Particles in the potential flow were advected according to the local velocity, and the drift volume was measured using the aforementioned axisymmetry assumption. The following section compares the kinematics and dynamics of the measured vortex flow and the computed potential flow.

3. Results

Figure 1 plots three frames from the computed flow corresponding to the passage of a sphere through a plane of Lagrangian particles in an ideal fluid. The particles exhibit looping paths referred to as *elasticas* by Milne-Thomson (1968). These trajectories result in a net downstream displacement of the particles and a distortion of the initial plane to a horn shape as previously observed by Darwin (1953), Lighthill (1956), Eames *et al.* (1994) and others. As mentioned previously, the volume of fluid between

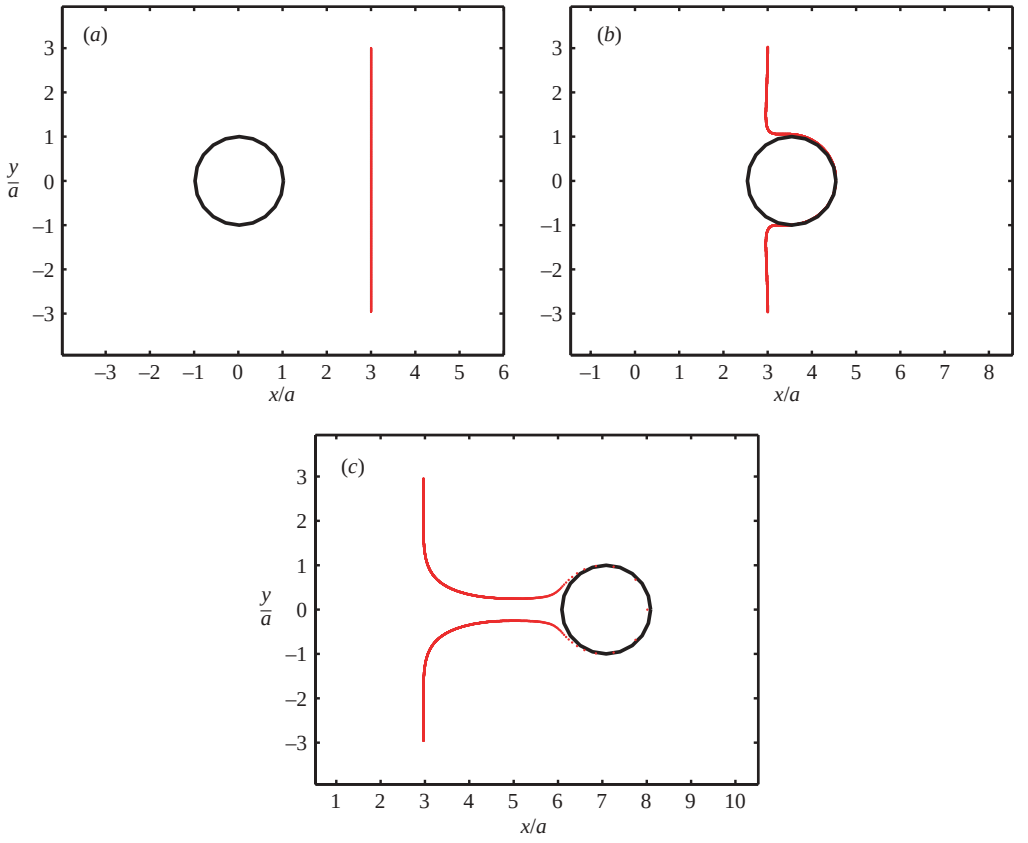

FIGURE 1. Passage of a solid sphere (black) through a plane of Lagrangian particles (red) in potential flow. Particle trajectories are computed from the exact solution in (2.1) and (2.2). (*a*) $Ut/a = 0$, (*b*) 3.6, (*c*) 7.2.

the distorted plane and its initial position has been shown by Darwin (1953) to equal the added-mass (per unit fluid density) of the solid sphere. This will be confirmed shortly. First let us compare these flow kinematics with those of the unidirectionally propagating vortex ring.

Figure 2 plots two frames from the measured flow corresponding to the passage of a vortex ring through a plane of Lagrangian particles initially located four cylinder radii downstream from the exit plane of the vortex generator. To visualize the location of the vortex ring in the flow, the frame transformation method of Dabiri & Gharib (2004) is implemented. The vortex ring boundary is indicated by the elliptical streamline containing the front and rear stagnation points. Shadden, Dabiri & Marsden (2005) recently confirmed the accuracy of the frame transformation method for determining the boundary of fully-formed vortex rings propagating via self-induction. Consistent with the results of the potential flow calculation of solid body motion, the Lagrangian particles exhibit looping elastica trajectories, which distort the initial plane into a horn shape. The particles pass along the vortex boundary in the same manner as the particles around the solid body in potential flow.

Despite the observed qualitative agreement between the induced Lagrangian drift behaviour of flow surrounding the solid body and the vortex, it is useful to further quantify the dynamics of the drift volume to determine if Darwin's (1953) method may

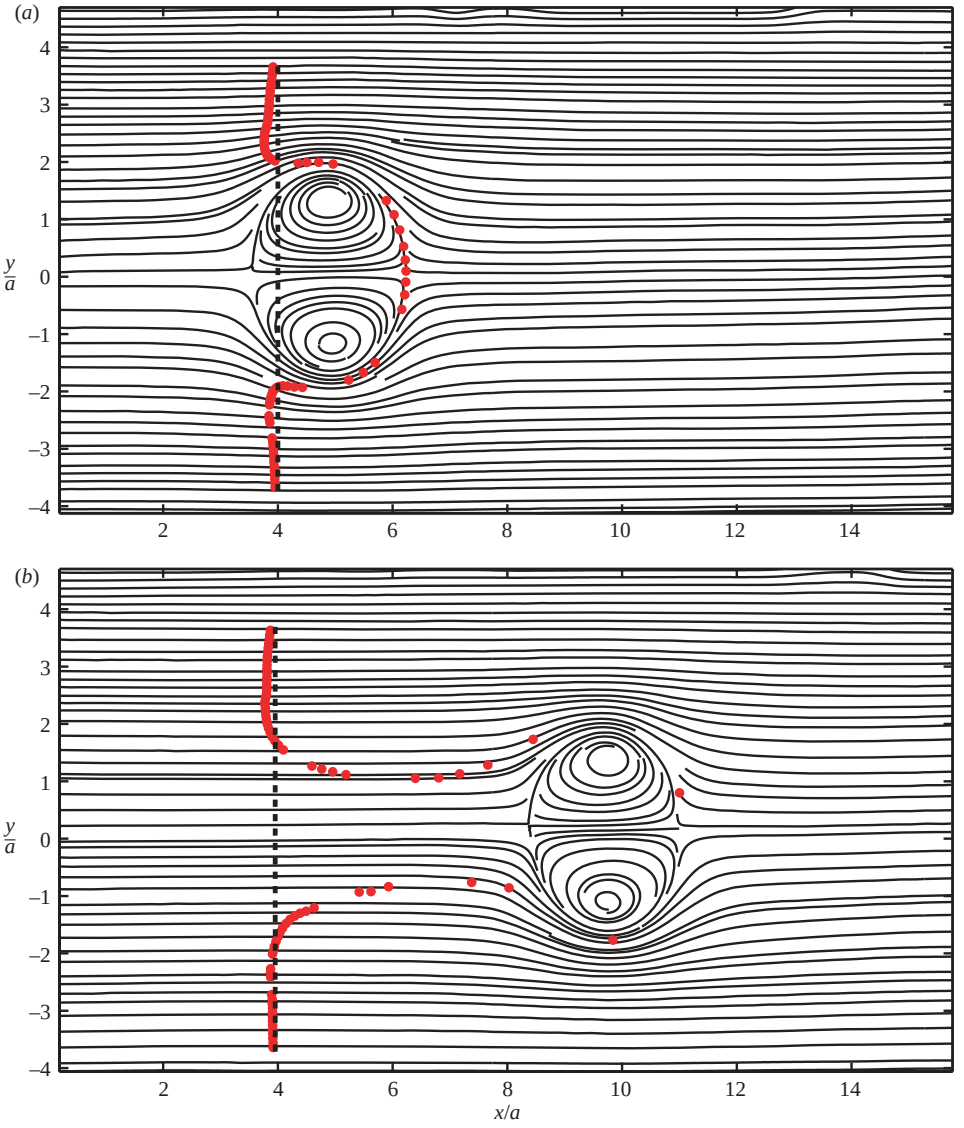

FIGURE 2. Passage of a vortex ring (shown in streamlines) through a plane of virtual Lagrangian particles (red) in the flow measured via DPIV. The vertical dashed line indicates the position of Lagrangian particles at $Ut/a = 0$. Particle trajectories are computed by updating their positions according to the measured time-dependent Eulerian velocity field. The parameters U and a in the dimensionless time are taken based on the average celerity of the vortex ring ($2.04\,\mathrm{cm\,s^{-1}}$) and the cylinder inner radius (1.27 cm), respectively. (*a*) $Ut/a = 4.9$, (*b*) 9.8.

be extended to include the propagation of vortices. Figure 3(*a*) plots the drift volume versus time for the solid sphere in potential flow as well as the measured vortex flow. The drift volume trends for several planes downstream of the vortex generator are plotted to determine the effect of the temporally varying vortex boundary (i.e. its growth due to fluid entrainment as it propagates downstream).

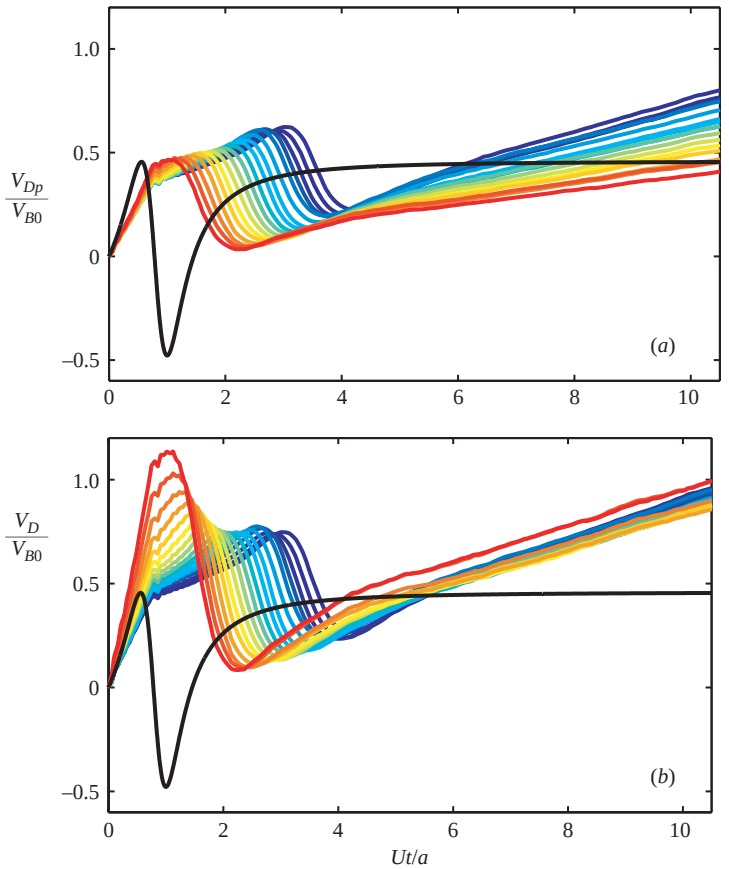

FIGURE 3. Drift volume versus time for computed and measured flows. The black line plots the drift volume of the computed potential flow around a propagating solid sphere. Coloured lines represent the drift volume of planes initially located in 0.3 cm increments from 2.7 cm (red) to 8.0 cm (blue) downstream of the vortex generator exit. The partial drift correction of Eames *et al.* (1994) is applied to the data in (*a*) to arrive at the data in (*b*).

In each case, the drift volume temporarily decreases as the body passes through the plane of Lagrangian particles. This effect reflects the looping elastica trajectory of the particles, which briefly experience induced motion in the upstream direction before continuing their downstream drift. As expected, the drift volume of the solid sphere in potential flow asymptotes to one-half of the sphere volume as $t \rightarrow \infty$. This behaviour corresponds with the known added-mass coefficient for a sphere propagating along the x-axis, i.e. $c_{xx} = 1/2$.

The drift volume of each plane in the measured vortex flow does not asymptote to a constant value as in the solid body case, but instead follows a linearly increasing trend as the vortex propagates downstream. This result is consistent with the prediction of the model flow computed by Turner (1964) for a temporally growing spherical vortex. However, before further analysing the experimental data, we must recognize that the initial and boundary conditions of Darwin's (1953) heuristic do not match those of the experiments. In particular, the vortices generated experimentally did not approach the Lagrangian particle planes from infinitely far upstream, nor is the radial extent of the particle planes infinite as required by Darwin (1953). This discrepancy

is resolved by implementing the concept of *partial drift* (Eames *et al.* 1994), which, in potential flows with no sources, accounts for the effects of a spatially finite Lagrangian plane and body approach distance on the measured drift volume. The ratio between the measured partial drift V_{Dp} and total drift V_D required by Darwin (1953) is given approximately by

$$\frac{V_{Dp}}{V_D} \approx -\frac{1}{2} + \frac{3}{2\sqrt{1+(r_L/d_0)^2}}, \tag{3.1}$$

where r_L is the finite radius of the Lagrangian plane being tracked and d_0 is the initial distance of approach between the propagating body and the Lagrangian plane (Eames *et al.* 1994). In the present measurements, the parameter d_0 has a different value for each plane downstream from the vortex generator exit plane. Hence, a different partial drift correction is applied to each plane. When equation (3.1) is applied to the measurements, the total drift of each plane becomes identical as the vortex moves downstream (figure 3*b*). This result suggests that the partial drift correction (3.1) has properly accounted for the finite initial approach distance between the vortex ring and each Lagrangian plane downstream of the vortex generator.

Notwithstanding this refinement of the data, the linearly increasing trend in the drift volume of the vortex flow persists. To account for this effect in a calculation of the vortex added-mass coefficient, let us first consider the definition of Darwin (1953):

$$c_{xx} = \frac{V_D}{V_B}. \tag{3.2}$$

Both the drift volume and the body volume are time-dependent for the vortex flow, and are also both augmented by the *net* entrainment of ambient fluid by the vortex (the entrainment and detrainment processes act simultaneously, cf. Maxworthy 1972). The effect of entrainment on the added-mass coefficient can be made explicit by rewriting (3.2) as

$$c_{xx} = \frac{V_D(t) - V_E(t)}{V_{B0} + V_E(t)}, \tag{3.3}$$

where V_{B0} is the initial body volume and V_E is the net volume of fluid entrained by the vortex. This latter term is subtracted from the numerator of (3.3) in accordance with the fact that Darwin's (1953) drift volume accounts for fluid external to the body that drifts in its direction of propagation. Although entrained fluid automatically contributes to the measured drift volume (i.e. since particles in the Lagrangian plane are entrained and carried downstream by the vorrtex; cf. Turner 1964), entrained fluid is a part of the body (*ipso facto*) and is therefore not a component of the external drifting fluid considered by Darwin (1953). To be sure, entrained fluid is the source of the time dependence of the body volume $V_B(t)$, as indicated by the denominator of (3.3). The absence of this contribution to the denominator would cause the added-mass coefficient to become undefined as $t \to \infty$, as observed by Turner (1964). Substituting for the entrained fluid volume in (3.3) using the fact that $V_E(t) = V_B(t) - V_{B0}$, a modified vortex added-mass coefficient can be defined:

$$c_{xx} = \frac{V_D(t)}{V_B(t)} + \frac{V_{B0}}{V_B(t)} - 1. \tag{3.4}$$

For a body of constant volume such as the solid sphere computed above, $V_B(t) = V_{B0}$ for all time t, leading to the cancellation of the second two terms and the recovery of Darwin's (1953) classical added-mass coefficient (3.2). When the body volume $V_B(t)$ increases monotonically, as in the vortex flow measured here, the second term

vanishes. In this case, the third term compensates the monotonic increase in drift volume $V_D(t)$ that occurs due to fluid entrainment. For the vortices generated here, $V_B(t) \sim 1.54t$. Dabiri & Gharib (2004) show that this measured growth rate is consistent with previous estimates of vortex ring entrainment (e.g. Liess & Didden 1976; Baird, Wairegi & Loo 1977). Combining this result with the measured trend in total drift volume in figure 3(*b*) ($V_D(t) \sim 2.65t$), the vortex added-mass coefficient as $t \to \infty$ is

$$c_{xx} = \frac{2.65}{1.54} - 1 = 0.72. \tag{3.5}$$

This is precisely the added-mass coefficient of a solid body with equivalent boundary geometry, where the aspect ratio of the measured vortex ring, $AR \approx 1.37$, was determined empirically using the frame transformation method of Dabiri & Gharib (2004). Hence, these experiments and analysis show both a qualitative and quantitative agreement between the added-mass behaviour of solid bodies in ideal flow and unidirectionally propagating vortices. Regardless of whether or not the vortex added-mass coefficient will always be identical to the value for an equivalent solid body in potential flow (e.g. for all components of the added-mass tensor), the result that deserves emphasis here is that there exists a well-defined vortex added-mass coefficient despite the fact that the vortex drift volume increases monotonically.

4. Discussion

The existence of a well-defined vortex added-mass coefficient has been demonstrated empirically. Fluid entrainment by the vortex is incorporated explicitly in the coefficient and the drift volume behaviour is found to be consistent with previous investigations. Although the existence of an added-mass effect associated with a fluid body is not unexpected (indeed, the potential flow solution for the solid body computed here is identical to the solution for the flow around Hill's spherical vortex), the existence of fluid entrainment by vortices has previously prevented the definition of a consistent, physically relevant vortex added-mass coefficient.

The analytical methods described here depend heavily on the ability to define boundaries for vortical motion in the fluid. The method of Dabiri & Gharib (2004) was sufficient for the simple vortex ring flow studied here; however, it cannot be extended to most flows of practical interest. Recent results by Haller (2005) and Shadden *et al.* (2005) have the potential to achieve the objective definition of vortex boundaries in more complex flows, facilitating application of the concepts introduced here.

The fact that the partial drift concept was effective here despite its formal validity for potential flows with no source suggests that it is also useful in practice for vortex flows with low entrainment rates (i.e. on the order of a few percent per second), such as the vortex rings studied here.

As derived by Saffman (1992, §4.2), the impulse required to set a region of fluid into unsteady vortical motion is given by

$$\boldsymbol{I} = \frac{1}{2}\int_{\boldsymbol{V}} \boldsymbol{x} \times \omega \, \mathrm{d}\boldsymbol{V} + \int_{\boldsymbol{S}} \phi \boldsymbol{n} \, \mathrm{d}\boldsymbol{s}, \tag{4.1}$$

where ω is the fluid vorticity and $\boldsymbol{n}$ is the unit normal vector directed into the region of compact vorticity. An important benefit of the vortex added-mass coefficient is that it can be used as a surrogate for the velocity potential ϕ in the second term, a parameter which is difficult to measure empirically. Since the first term is much

easier to measure experimentally, it has often been used by itself for force estimates in unsteady wake analyses and studies of fluid–structure interaction such as vortex-induced vibrations. However, recent studies of unsteady vortex flows suggest that the second term of equation (4.1) can be quite substantial (e.g. Krueger & Gharib 2003; Dabiri 2005); therefore, the development of techniques to infer its contribution in fluid flows is necessary in order to avoid underestimation of unsteady fluid forces. The vortex added-mass concept introduced here provides one such technique.

REFERENCES

Adrian, R. J. 1991 Particle-imaging techniques for experimental fluid-mechanics. *Annu. Rev. Fluid Mech.* **23**, 261–304.

Baird M. H. I., Wairegi T. & Loo H. J. 1977 Velocity and momentum of vortex rings in relation to formation parameters. *Can. J. Chem. Engng* **55**, 19–26.

Benjamin, T. B. 1986 Note on added mass and drift. *J. Fluid Mech.* **169**, 251–256.

Bush, J. W. M. & Eames, I. 1998 Fluid displacement by high Reynolds number bubble motion in a thin gap. *Intl J. Multiphase. Flow* **24**, 411–430.

Dabiri, J. O. 2005 On the estimation of swimming and flying forces from wake measurements. *J. Expl Biol.* **208**, 3519–3532.

Dabiri, J. O. & Gharib, M. 2004 Fluid entrainment by isolated vortex rings. *J. Fluid Mech.* **511**, 311–331.

Darwin, C. 1953 Note on hydrodynamics. *Proc. Camb. Phil. Soc.* **49**, 342–354.

Eames, I. 2003 The concept of drift and its application to multiphase and multibody problems. *Phil. Trans. R. Soc. Lond.* A **361**, 2951–2965.

Eames, I., Belcher, S. E. & Hunt, J. C. R. 1994 Drift, partial drift and Darwin's proposition. *J. Fluid Mech.* **275**, 201–223.

Eames, I. & Duursma, G. 1997 Displacement of horizontal layers by bubbles injected into fluidized beds. *Chem. Engng Sci.* **52**, 2697–2705.

Eames, I. & Flór, J.-B. 1998 Fluid transport by dipolar vortices. *Dyn. Atmos. Oceans* **28**, 93–105.

Haller, G. 2005 An objective definition of a vortex. *J. Fluid Mech* **525**, 1–26.

Krueger, P. S. & Gharib, M. 2003 The significance of vortex ring formation to the impulse and thrust of a starting jet. *Phys. Fluids* **15**, 1271–1281.

Liess, C. & Didden, N. 1976 Experimente zum Einfluss der Anfangsbedingungen auf die Instabilität von Ringwirblen. *Z. Angew. Math. Mech.* **56**, T206–T208.

Lighthill, M. J. 1956 Drift. *J. Fluid Mech.* **1**, 31–53.

Maxworthy T. 1972 The structure and stability of vortex rings. *J. Fluid Mech.* **51**, 15–32.

Milne-Thompson, M. 1968 *Theoretical Hydrodynamics.* Dover.

Saffman, P. G. 1992 *Vortex Dynamics.* Cambridge University Press.

Shadden, S. C., Dabiri, J. O. & Marsden, J. E. 2005 Lagrangian analysis of entrained and detrained fluid in vortex rings. *Phys. Fluids* (submitted).

Turner, J. S. 1964 The flow into an expanding spherical vortex. *J. Fluid Mech.* **18**, 195–208.

Willert, C. E. & Gharib, M. 1991 Digital particle image velocimetry. *Exps. Fluids* **10**, 181–193.

Yih, C.-S. 1997 Evolution of Darwinian drift. *J. Fluid Mech.* **347**, 1–11.